Effects of various hydrogenated temperatures on photocatalytic activity of mesoporous titanium dioxide

Chan Wai Soo[1], Chin Wei Lai[1], Guan-Ting Pan[2], Thomas Chung-Kuang Yang[2], Kian Mun Lee[1], Rahimi Muhammad Yusop[3], Joon Ching Juan[1,4] ✉

[1]*Nanotechnology and Catalysis Research Centre (NANOCAT), IPS Building, University of Malaya, Kuala Lumpur, Malaysia*
[2]*Department of Chemical Engineering, National Taipei University of Technology, Taipei City, Taiwan*
[3]*School of Chemical Sciences and Food Technology, Faculty of Science and Technology, National University of Malaysia, UKM, 43600 Bangi, Selangor Darul Ehsan, Malaysia*
[4]*School of Science, Monash University Malaysia Campus, School of Science, Bandar Sunway 46150, Malaysia*
✉ *E-mail: jcjuan@um.edu.my*

Published in Micro & Nano Letters; Received on 4th May 2017; Revised on 5th July 2017; Accepted on 14th August 2017

Hydrogenated titanium dioxide (H-TiO_2) has drawn much research attention in the photocatalysis society since it has significantly improved solar absorption and enhanced photocatalytic activity. Nevertheless, the key factor that leads to the enhanced photocatalytic performance of H-TiO_2 is still debatable. To clarify this issue, the structural properties of H-TiO_2 and its effects on photogenerated charges are investigated. Mesoporous H-TiO_2 was subjected to different hydrogenation temperatures rate under the flow of purified H_2 gas and its photocatalytic activities are evaluated by reactive black 5 photodegradation. The H-TiO_2 pretreated at different temperatures seems to have a detrimental effect on photocatalytic activity as compared with that of untreated H-TiO_2. Further investigations reveal that H-TiO_2 treated at high temperature can cause the formation of less photoactive rutile phase and agglomeration that leads to the inhibition of their photocatalytic activity.

1. Introduction: Titanium dioxide (TiO_2) is an interesting photoactive material which is capable of providing useful photocatalytic applications such as the degrading of organic pollutants [1]. Since the discovery of TiO_2 roles in photoelectrochemical splitting of water made by Fujishima and Honda [2], Frank and Bard [3, 4] have reported that TiO_2 is capable to reduce CN^- in water which marked the first usage of TiO_2 as a remedy for environmental pollutants. These exciting breakthroughs in the past have driven the research directions toward TiO_2 with the hope to exploit solar energy for treating environmental contaminants. In particular, TiO_2 has been the best known and most widely used photocatalytic material owing to its photo-stability, environmentally friendly and cost effectiveness [5]. The potential of TiO_2 applications have been limited by several main factors which includes a wide bandgap about 3.2 eV which is confined to the photoactivation of TiO_2 within the range of wavelength which is shorter than 400 nm. This is usually associated with the usage of ultraviolet (UV) light irradiation only and the rapid recombination rate of photogenerated electron–hole pairs that are useful in creating radicals for decomposing organic contaminants. To circumvent the limitations posed by TiO_2, tremendous efforts have been exerted to improve the effectiveness of TiO_2 such as doping TiO_2 with cations (Fe, Cu, Cr, V, Mn, Ni, Co and Zn) [6–13] or anions (N, F, Cl, S and P) [14–19] and incorporating the defects into TiO_2 crystals [20]. The cation doping seems to be an effective technique to enhance the photocatalytic activity.

Among the techniques of tailoring the bandgap of TiO_2, reduced TiO_2 prepared via hydrogen treatment has gained wide attention. Chen *et al.* [21] reported that they have successfully synthesised unique black anatase TiO_2 nanoparticles through hydrogenation under 20 bar of hydrogen pressure at 200°C for 5 days. These black TiO_2s have shown an improved optical absorption from UV light up to near infrared zone with a narrowed bandgap of 1.0 eV. These hydrogenated TiO_2 (H-TiO_2) which are usually exhibited in grey or black colour have shown excellent photocatalytic activity performance in the degradation of organic pollutants [22]. On the basis of scientific literature dealing with H-TiO_2 [21–27], it is inferred that there exists crucial uncertainties about the resulting photocatalytic activity. Some researchers claim that the photocatalytic of H-TiO_2 samples are better than that of pristine TiO_2 (P-TiO_2) [28–30]. In contrast, some studies [24, 31, 32] have shown that hydrogenation not only failed to improve the efficiency of TiO_2 but also caused a drop in the activity depending on the degree of hydrogenation. For example, Yu *et al.* [26] conducted some studies on the hydrogenation on white anatase TiO_2 powder by flowing 50 ml/min of H_2 at atmospheric pressure for 0.5–1 h at the temperature range of 500–700°C and found out that hydrogenation can effectively improve the photocatalytic efficiency of TiO_2. On the other hand, Leshuk *et al.* [24] conducted a study on hydrogenated TiO_2 under 20 bar H_2 for 24 h at various temperatures (250, 350 and 450°C) and found that the hydrogenation has an inhibitory effect on the photocatalytic activity of TiO_2 where the poor performance might be attributed to the formation of bulk defects at high temperature of hydrogenation treatment. Hence, the annealing temperature during hydrogenation treatment plays a crucial role in photocatalytic activity of H-TiO_2.

In spite of the existence of the seemingly contradictory results, research in the field of photocatalytic activity of H-TiO_2 is still interesting and valuable. Despite the fact that hydrogenation is capable of tuning the absorption of TiO_2 into visible (vis) light as well as infrared region depending on the hydrogenation level, there is a lack of study on H-TiO_2 under artificial sunlight irradiations after treated at different elevated hydrogenation temperatures. Most of the studies that were reported earlier have been conducted by selectively hydrogenating TiO_2 and then carried out their photocatalytic activity in the presence of UV or vis light radiation. Moreover, the influence of thermal hydrogenation in mesoporous TiO_2 and its photocatalytic has not been investigated. Hence, the aim of this Letter is to investigate the effect of annealing temperature on the photocatalytic behaviour of mesoporous H-TiO_2 under artificial solar light (UV–vis). In addition, the impact of hydrogenation on various properties such as crystallography structure, particle size, surface area, pore size, pore volume, morphology and charge carriers recombination rate and bandgap of H-TiO_2 was also evaluated.

2. Materials and methods

2.1. Material and synthesis: Ti (IV) tetra-isopropoxide (TTIP) (97%) and Pluronic® F127 were purchased from Sigma-Aldrich, hydrochloric acid (HCl) (37%, analytical grade) was supplied by Merck and ethanol (96%) provided by Fisher Scientific were used without further purification. In a typical procedure [21], a precursor of acidic aqueous solution was prepared by dissolving an organic template, Pluronic F127 in a mixture of ethanol and deionised water followed by addition of HCl. Afterwards, TTIP as the Ti precursor was added dropwise into the acidic mixture of precursor under stirring. The molar ratios of TTIP/F127/HCl/H_2O/ethanol were set at 1:0.005:0.5:15:40. The resultant transparent solution was kept under stirring for 24 h at 45°C. After that, the precipitates were washed with deionised water and ethanol prior drying in oven at 85°C for 24 h. The dried TiO_2 powders were then calcined in tubular furnace at 500°C for 6 h with a ramping rate of 0.5°C/min. Then, these TiO_2 powders were treated separately under a purified H_2 gas flow of 10 ml/min at atmospheric pressure at elevated temperature ranging from 300 to 700°C and denoted as H-TiO_2.

2.2. Characterisation: The crystallography structure of the synthesised H-TiO_2 samples were analysed by employing Bruker D8 advanced diffractometer operated at 40 kV and 30 mA with Cu Kα radiation ($\lambda = 0.15406$ nm) for phase identification through a scanning range from $2\theta = 10°$ to 80° at a step size of 0.02° s^{-1}. The bandgap energy for each H-TiO_2 sample was determined by the Kubelka–Munk function from the measurement of its optical absorption in the range of 200–800 nm by using a Varian Cary 100 diffuse reflectance UV–vis spectrophotometer (DR–UV–vis). Both Raman and photoluminescence spectra for H-TiO_2 were obtained by using a Renishaw inVia Raman microscope with a laser (514 nm, 5 mW) focused onto a microsised spot (1 µm). A high-resolution transmission electron microscopy (HRTEM) analysis were carried out by using a JEOL JEM-2100F electron microscope at an acceleration voltage of 200 kV to observe the effect of thermal hydrogenation on the morphologies and microstructures of the H-TiO_2 images. The HRTEM samples were prepared by sonication of the powders in ethanol for 15 min and subsequently the dispersion was dropped onto carbon copper grids. A nitrogen absorption–desorption isotherm measurement was conducted on a Micromeritics TriStar II 3020 surface area and porosity analyser at 77 K. Before each measurement, H-TiO_2 sample was degassed at 300°C for 4 h. The specific surface area of H-TiO_2 was determined by using Brunauer–Emmett–Teller (BET) theory and Barrett–Joyner–Halenda (BJH) method and was used to measure pore size distributions and pore volumes of the samples.

2.3. Photocatalytic activity: The photocatalytic activity of H-TiO_2 samples was studied by measuring the degradation of reactive black 5 (RB5) under artificial sunlight irradiation. A 30 mg of H-TiO_2 powder was dispersed in 100 ml of 10 mg/l of RB5 dye. Prior to light irradiation, the suspension was stirred for 30 min in the dark to achieve adsorption–desorption equilibrium with the photocatalyst. A 150 W xenon arc lamp (200–2500 nm, Newport) surrounded by a circulating water jacket for cooling purpose was used as the light source to represent one sun. After the light source was turned on, at given intervals, about 5 ml of samples was taken out and filtered by using a disposable syringe filter to remove the photocatalyst particles. Then, the photocatalytic activity for each H-TiO_2 samples can be determined from the RB5 photodegradation efficiency by measuring the remaining concentration of RB5 through the analysis of UV–vis absorbance from a spectrophotometer at the wavelength of 597 nm. The percentage of removal is calculated by using simple equation as below:

$$\%\text{removal efficiency} = 100 \times \left(\frac{c_0 - c}{c_0}\right) \tag{1}$$

where C_0 is the initial concentration of dye solution and C is the concentration of the dye solution after photoirradiation.

The kinetics of the disappearance of RB5 was also considered. Generally, the disappearance of dye follows a pseudo-first-order kinetics and several studies proved to have the same pattern [33–35]. Henceforth, the colour degradation of RB5 for this research was fitted to a pseudo-first-order kinetic model with respect to the dye's concentration, that is

$$\ln\left(\frac{C}{C_0}\right) = -kt \tag{2}$$

where C (mg/l) is the dye concentration at t, C_0 (mg/l) is the initial dye concentration, t (min) is the reaction time and k (min^{-1}) is the pseudo-first-order rate constant.

3. Results and discussion

3.1. Crystallinity and morphology: The changes of crystal structures for H-TiO_2 during the thermal hydrogenation process were determined by X-ray diffraction (XRD) spectra (Fig. 1.). The results indicated that H-TiO_2 underwent a significant phase change from dominant anatase to rutile with the increment of hydrogenation temperature as compared with the synthesised P-TiO_2 which demonstrated a major anatase phase coexisting with a small amount of rutile phase. The characteristic diffraction peaks of anatase phase TiO_2 were detected at $2\theta = 25.3°$, 37.9°, 48.1°, 54.0°, 55.2° and 62.8° which correspond to (101), (004), (200), (105), (211) and (204) crystal surface. This implies that the observed diffractions that are attributable to anatase TiO_2 are in good accordance with those in the standard JCPDS Card No. 21-1272 [36]. It is observed that the hydrogenation temperature can affect the ratio of anatase and rutile phase. As the hydrogenation temperature increases from 300 to 700°C, the crystallinity of dominant anatase peak at (101) has decreased while the rutile becomes the sole phase in H-TiO_2. The anatase phase was completely transformed into rutile phase at 700°C under hydrogenation. This is expected by many researchers [1, 37] that anatase tends to transform into rutile when temperature is more than 500°C. Several diffraction peaks for rutile TiO_2 at 2θ values of 27.58°, 36.30°, 41.30°, 54.42°, 62.86° and 65.66° are assigned to (110), (101), (111), (211), (002) and (211) planes (JCPDS Card No. 21-1276) are observed in H-TiO_2,

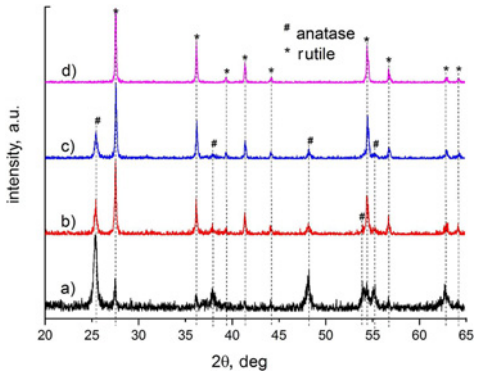

Fig. 1 *XRD spectra of*
a P-TiO_2
b 300°C H-TiO_2
c 500°C H-TiO_2
d 700°C H-TiO_2

doi: 10.1049/mnl.2017.0238

Table 1 Textural properties of pristine TiO_2 and H-TiO_2 at various hydrogenation temperatures

Catalyst	Anatase					Rutile							
	Lattice parameters		Unit cell volume, Å^3	Crystallite size[a], nm	Ratio X_A^b, %	Lattice parameters		Unit cell volume, Å^3	Crystallite size[a], nm	Ratio X_R^b, %	BET surface area[c], m^2/g	Cumulative volume[d], cm^3/g	Average pore width, nm
	$a=b$, Å	C, Å				$a=b$, Å	c, Å						
pristine TiO_2	3.784	9.493	135.97	21.6	63.0	4.586	2.959	62.24	34.4	37.0	73.9	0.147	59.1
300°C H-TiO_2	3.780	9.491	135.62	28.9	63.0	4.582	2.957	62.08	46.3	77.9	16.7	0.120	24.3
500°C H-TiO_2	3.776	9.482	135.19	26.4	22.1	4.581	2.956	62.03	51.3	81.2	14.4	0.116	24.7
700°C H-TiO_2	—	—	—	—	18.8	4.580	2.955	62.00	61.1	100.0	4.75	0.042	37.7

[a]Crystallite sizes were estimated by using Scherrer's formula.
[b]Crystal phase ratios were calculated by using Spurr's equation.
[c]Surface area determined by BET.
[d]Pore volume was calculated based on BJH.
[e]Average pore width was based on BJH.

whereas the characteristic peak of brookite ($2\theta=30.8°$) are not detected in all of the samples [38].

The lattice parameters (a, c) of the tetragonal unit cell for H-TiO_2 are determined by using the relationship of $a=b=2\times d_{004}$ and $c=4\times d_{200}$ for anatase phase through the selection of XRD peaks at crystal plane (004) and (200), whereas the faces of (200) and (002) are chosen for the rutile structure, where $a=b=2\times d_{004}$ and $c=2\times d_{200}$ applied. The crystallite size, crystal phase ratio and lattice parameters of H-TiO_2 samples are shown in Table 1. From Table 1, the unit cell volume and lattice parameters (a and c) for both anatase and rutile generally decrease with the increase of hydrogenation temperature. This result is in concordance with the previous study [39, 40], in which the unit cell volume of TiO_2 will contract after hydrogenation. It has been reported that hydrogenation of TiO_2 at high temperature increased the crystallite size, where thermal treatment can induce the TiO_2 grain growth [27].

The morphology and structural changes of the H-TiO_2 samples were characterised by HRTEM. Figs. 2*a–d* show the HRTEM images of pristine TiO_2 and H-TiO_2 with a difference in the degree of hydrogenation temperature. As seen from Fig. 2*a*, pristine TiO_2 demonstrated a framework of highly crystalline TiO_2 with clear lattice fringe and a spacing of 0.35 nm between the (101) planes of anatase phase. However, after hydrogenation, a disordered layer can be observed at the edge of H-TiO_2 lattice, where the blurred images indicated the distortion of TiO_2 structure which can be attributed to the effect of hydrogenation treatment [41]. At 300°C of hydrogenation temperature, a disordered layer (0.8–2.2 nm) was formed on the surface of TiO_2 (Fig. 2*b*). A further increment of the hydrogenation temperature, the thickness of the disordered layer was increased to 1.9–2.7 and 2.1–4.3 nm at 500 and 700°C, respectively. The interplanar spacing of 0.32 nm corresponding to the (110) crystal planes of rutile TiO_2 was observed in the H-TiO_2 samples, which are the dominant crystal phase as shown by the crystal phase ratio calculation from XRD.

To further investigate the structural changes of TiO_2 after subjected to different degrees of thermal hydrogenation treatment, Raman spectroscopy is sensitive in detecting the disordered phase. As shown in Fig. 3, P-TiO_2 exhibited four typical anatase Raman bands at 144 cm^{-1} (E_g), 397 cm^{-1} (B_1g), 516 cm^{-1} (A_1g+B_1g) and 637 cm^{-1} (E_g) [42] while the characteristic bands of rutile at 446 cm^{-1} (E_g) and 609 cm^{-1} (A_1g) [43] appeared from 300°C H-TiO_2 and became dominant at a higher hydrogenation temperature. These results are in concordance with the XRD data, where the H-TiO_2 undergoes phase changes due to the increase of hydrogenation temperature and these can be seen from the weakening of anatase Raman peaks with the increasing of rutile Raman peaks. It can also be observed that the Raman peaks

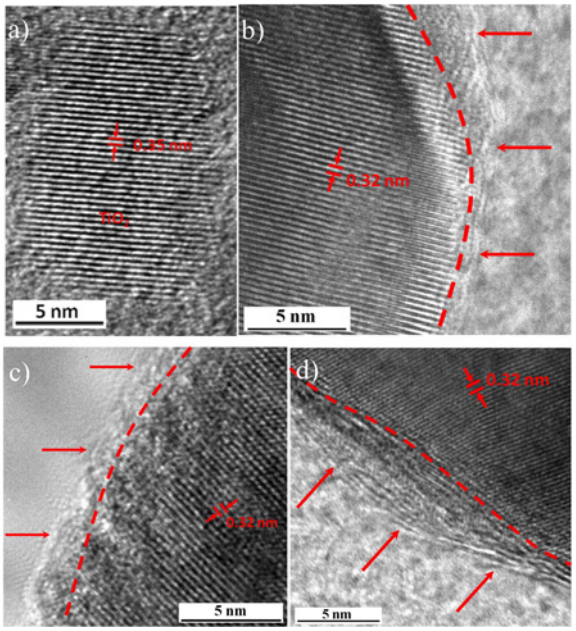

Fig. 2 *HRTEM images of*
a P-TiO_2 and H-TiO_2 heated at different temperatures
b 300°C
c 500°C
d 700°C

for H-TiO_2 had slightly blue shifted from 144 (TiO_2) to 146 cm^{-1} (H-TiO_2) as the hydrogenation temperature increased from 300 to 700°C. This phenomenon had concurred with several studies [26, 44], in which the blue shifted of Raman peaks were the characteristics of the existence of the disordered phase and the cause of the shift is due to the presence of defects such as oxygen vacancies. These results are consistent with the observation of distorted lattice fringe in HRTEM images of H-TiO_2.

3.2. Optical properties and surface area: The optical absorbance of P-TiO_2 and H-TiO_2 samples were determined by DR–UV–vis spectroscopy. Fig. 4 shows the UV–vis spectra of P-TiO_2 and H-TiO_2 prepared at various hydrogenation temperatures. It can be observed that hydrogenation of TiO_2 increased the absorption of the vis light and in the infrared region but it only has little effect on the light absorption ability in the UV range as compared with the P-TiO_2. The bandgap of the entire hydrogenated sample from 300 to 700°C was similar at 2.96–2.97 eV. This demonstrated

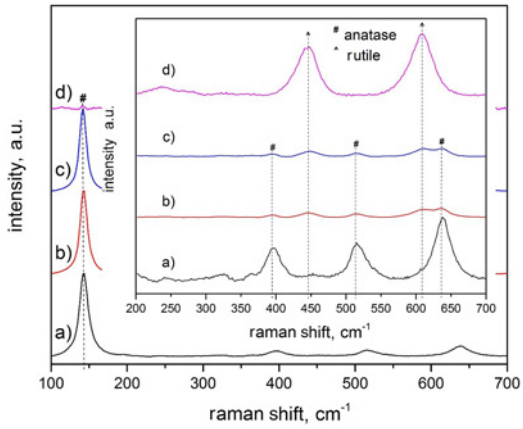

Fig. 3 *Raman spectra of*
a P-TiO_2
b 300°C H-TiO_2
c 500°C H-TiO_2
d 700°C H-TiO_2

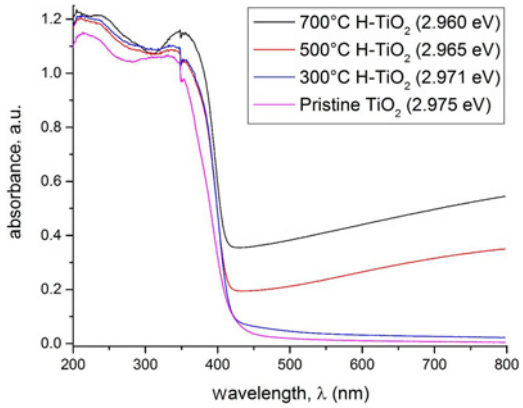

Fig. 4 *UV–vis absorption spectra of P-TiO_2 and H-TiO_2 at different temperatures*
Note: The parenthesis indicate the bandgap calculated by Kubelka–Munk function

that the hydrogenation did not have much effect on the bandgap. As the hydrogenation temperature increased from 300 to 700°C, the vis light and infrared absorption efficiencies increased. This indicated that more electron–hole pairs can be generated under vis light irradiation leading to the enhancement of photocatalytic activity. The strong vis light and infrared absorption can be attributed to the formation of more oxygen vacancies associated with Ti^{3+} ions in the higher hydrogenation temperature [29]. However, the crystal phase of TiO_2 tended to change at high hydrogenation temperature as shown in XRD and Raman spectra, thus the destruction of crystallite structure is imminent.

The synthesised P-TiO_2 powder changed from its original white to slightly yellowish colour at the early stage (300°C) of hydrogenation temperature. With the higher hydrogenation thermal treatments (>500°C), the colouration of the H-TiO_2 samples started to become bluish and gradually changed into grey as shown in Fig. 5. The hydrogenation temperature has impact on the colour changes of TiO_2. They are due to the reduction of P-TiO_2 and the formation of Ti^{3+} ions by electron trapping at the Ti^{4+} centres, where the colour of the H-TiO_2 samples can indicate the amount of Ti^{3+} ions up to a certain extent [45]. The darker colour of H-TiO_2 can be obtained by further increasing the hydrogenation temperature, and thus indicating that the Ti^{3+} ions can be controlled by modifying the hydrogenation temperature.

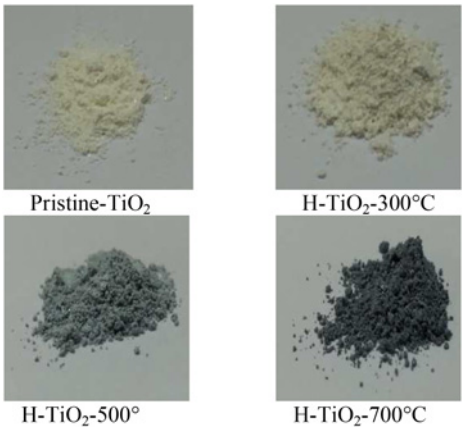

Fig. 5 *Photograph of H-TiO_2 samples prepared with a H_2 gas flow at temperatures of 300–700°C. Gradual changes in colour from white to grey to a different degree are observed, depending on annealing temperatures*

Fig. 6 shows the N_2 adsorption–desorption isotherm curves of the P-TiO_2 and H-TiO_2 after hydrogenation at 300, 500 and 700°C. It can be seen that most of the samples follow the type IV isotherm which indicated the presence of mesopores (2–50 nm). Observation indicates that the hysteresis loops shifted from 0.5–0.8 $p/p°$ to a higher relative pressure range ($p/p° = 1$) and the areas of the hysteresis loops decreased with the increase of hydrogenation temperature. This concurred with other study [46] that hydrogenation at high temperature can lead to the decrease of pore volume and an increase of average pore size of H-TiO_2. The hysteresis loops of 700°C H-TiO_2 which are hard to observe indicated some pore collapse during high temperature of hydrogenation. It can be seen that hydrogenation temperature plays a significant role in affecting the pore size distribution and effective surface area for TiO_2. The S_{BET} and cumulative pore volume with average pore size of P-TiO_2 and H-TiO_2 are presented in Table 1. The pore size distribution curve (as shown at the inset of Fig. 6) slowly shifts to the macropore region and the pore volume decrease as well after subjected to different degrees of hydrogenation temperature. In general, large surface area will give a better

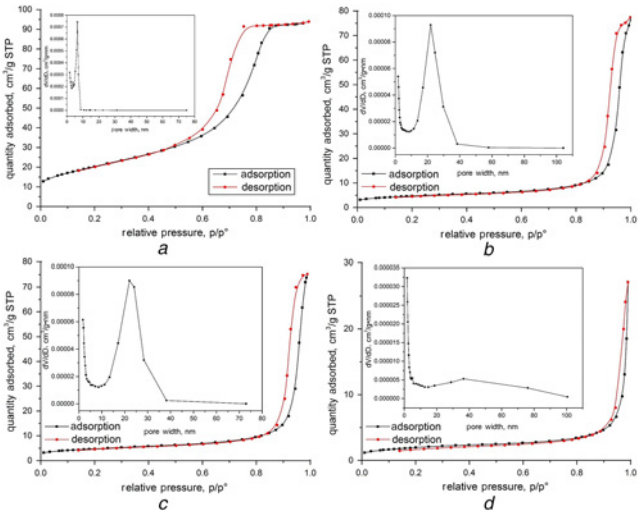

Fig. 6 *Nitrogen adsorption–desorption isotherms and pore size distribution (inset) of*
a P-TiO_2 and H-TiO_2 after hydrogenation at
b 300°C
c 500°C
d 700°C for 12 h

doi: 10.1049/mnl.2017.0238

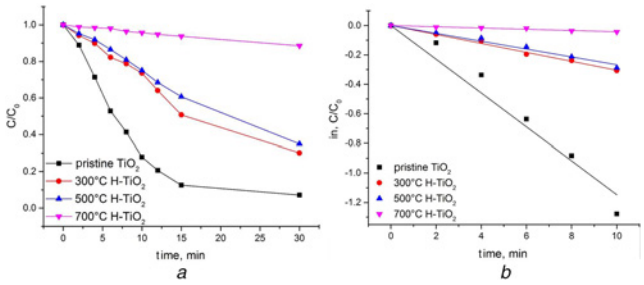

Fig. 7 *Rate of photocatalytic degradation of RB5 under artificial sunlight*
a Photodegradation of RB5 by H-TiO_2 as a function of irradiation time
b Kinetics of RB5 removal by H-TiO_2 with different hydrogenation temperatures against time

photocatalytic activity. In this Letter, high heating temperature during hydrogenation of TiO_2 has greatly reduced the surface area [47, 48]. The average pore size is connected with the TiO_2 crystallite size, where the increase of crystallite size will lead to the increase of average pore size [49, 50]. This is in good agreement with the XRD analysis, where both the crystallite size and average pore size for rutile phase of H-TiO_2 increase with the rising of hydrogenation temperature.

3.3. Photocatalytic degradation of RB5: Photocatalytic degradation of RB5 was carried out by utilising H-TiO_2 under artificial solar light. In this work, we have studied the effect of hydrogenation temperature in affecting the photocatalytic activity of H-TiO_2. Fig. 7*a* shows the photodegradation efficiency of P-TiO_2 and H-TiO_2 increased with time under artificial sunlight illumination. As compared to the P-TiO_2, high temperature of hydrogenation onto TiO_2 has caused detrimental effect on the photocatalytic activity of TiO_2. It was observed that P-TiO_2 managed to completely photodegrade RB5 at 60 min and gives the highest rate constant. Fig. 7*b* indicated that all samples follow pseudo-first-order kinetics, in which the rate constant k values of RB5 decreased in the order of P-TiO_2 ($0.115\ min^{-1}$) > 300°C H-TiO_2 ($0.0305\ min^{-1}$) > 500°C H-TiO_2 ($0.0267\ min^{-1}$) > 700°C H-TiO_2 ($0.00425\ min^{-1}$) with $R^2 \geq 0.98$.

With the increase of hydrogenation temperature, the photocatalytic activity of H-TiO_2 decreased gradually. It is notable that P-TiO_2 managed to achieve 93% of RB5 photocatalytic degradation, while the H-TiO_2 samples exhibit a weaker photocatalytic activity. This can be attributed to the decrease of specific surface area of H-TiO_2 due to agglomeration on high temperature of hydrogenation treatment which is in concordance with the BET surface area. A low surface area will contain less active sites that hindered the photoreactivity [51]. Several studies has also concurred that hydrogenation of TiO_2 will lead to the decrease of specific surface area [24, 27]. Besides that, XRD and Raman spectra have also shown that at high temperature of hydrogenation treatment, it will lead to the formation of rutile phase. Therefore, this will also cause the loss of photocatalytic activity. This is because it is well known that rutile has a direct bandgap, in which the photo-excited electrons recombine directly with holes, thus decreasing the photogenerated electron–hole pairs lifetime [52]. Hence, the overall photocatalytic activity of H-TiO_2 decreases with the increase of hydrogenation temperature. This result is in concordance with the previous literatures, where hydrogenation of TiO_2 can be counterproductive in improving the photocatalytic activity of TiO_2 [24, 31].

4. Conclusions: A series of H-TiO_2 hydrogenated at different temperatures were successfully synthesised. Their photocatalytic degradation of RB5 was evaluated under artificial sunlight irradiation. It was notable that P-TiO_2 has the best photocatalytic activity compared with H-TiO_2 pretreated at different temperatures. Although UV–vis absorption spectra indicates that H-TiO_2 samples have broad absorption ranges from UV to near infrared zone, the photocatalytic activity decreases due to the lower surface area and formation of rutile phase. The presence of less photoactive rutile phase and extremely low specific surface area of H-TiO_2 has significantly inhibited the performance of photocatalytic degradation of RB5, where the less active site are available for the substrate to be absorbed on the surface of the photocatalyst, where the photodegradation of it can be occurred. Thus, the overall photocatalytic performance of H-TiO_2 at high hydrogenation temperature has dropped.

5. Acknowledgment: The authors greatly acknowledge the financial support received under MOSTI e-science Fund (06-01-03-SF0949), the Transdisciplinary Research Grant Scheme (TR001B-2015A) and the Postgraduate Research Grant (PPP) grant (PG061-2013B). The authors to thank the University of Malaya for the UM fellowship scheme (SBUM).

6 References

[1] Hanaor D.A.H., Sorrell C.C.: 'Review of the anatase to rutile phase transformation', *J. Mater. Sci.*, 2011, **46**, pp. 855–874
[2] Fujishima A., Honda K.: 'Electrochemical photolysis of water at a semiconductor electrode', *Nature*, 1972, **238**, pp. 37–38
[3] Frank S.N., Bard A.J.: 'Heterogeneous photocatalytic oxidation of cyanide and sulfite in aqueous solutions at semiconductor powders', *J. Phys. Chem.*, 1977, **81**, pp. 1484–1488
[4] Frank S.N., Bard A.J.: 'Heterogeneous photocatalytic oxidation of cyanide ion in aqueous solutions at TiO_2 powder', *J. Am. Chem. Soc.*, 1976, **99**, pp. 303–304
[5] Zhu L.Y., Liu X.T., Qin W.W., *ET AL.*: 'Preparation, characterization and electronic structures of Fe-doped Tio_2 nanostructured fibers', *Mater. Res. Bull.*, 2013, **48**, pp. 2737–2745
[6] Qamar M., Merzougui B., Anjum D., *ET AL.*: 'Synthesis and photocatalytic activity of mesoporous nanocrystalline Fe-doped titanium dioxide', *Catal. Today*, 2014, **230**, pp. 158–165
[7] Gas D.X.M.-V., La Rosa J.R.D., Lucio-Ortiz C.J., *ET AL.*: 'Photocatalytic degradation of trichloroethylene in a continuous annular reactor using Cu-doped Tio_2 catalysts by sol–gel synthesis', *Appl. Catal. B, Environ.*, 2015, **179**, pp. 249–261
[8] Yadav H.M., Kolekar T.V., Barge A.S., *ET AL.*: 'Enhanced visible light photocatalytic activity of Cr_3+-doped anatase Tio_2 nanoparticles synthesized by sol–gel method', *J. Mater. Sci. Mater. Electron.*, 2016, **27**, pp. 526–534
[9] Jabbari V., Hamadanian M., Reisi-Vanani A., *ET AL.*: 'V-codoped TiO_2 nanocomposite prepared via a photochemical reduction technique as a novel high efficiency visible-light-driven nanophotocatalyst', *RSC Adv.*, 2015, **5**, pp. 78128–78135
[10] Kuzmicheva G.M., Savinkina E.V., Obolenskaya L.N., *ET AL.*: 'Synthesis of Mn-sensitized TiO_2 nanoparticles: influence of sequence of reagents on phase composition and photocatalytic activity', *J. Nanoparticle Res.*, 2015, **17**, pp. 1–12
[11] Chen C.-Y., Hsu L.-J.: 'Kinetic study of self-assembly of Ni (II)-doped TiO_2 nanocatalysts for the photodegradation of azo pollutants', *RSC Adv.*, 2015, **5**, pp. 88266–88271
[12] Zhao C., Shu X., Zhu D., *ET AL.*: 'High visible light photocatalytic property of Co_2^+-doped TiO_2 nanoparticles with mixed phases', *Superlattices Microstruct.*, 2015, **88**, pp. 32–42
[13] Benjwal P., Kar K.K.: 'Removal of methylene blue from wastewater under a low power irradiation source by Zn, Mn co-doped TiO_2 photocatalysts', *RSC Adv.*, 2015, **5**, pp. 98166–98176
[14] Fang Q., Tang J., Zou H., *ET AL.*: 'Preparation of N-Doped mesoporous TiO_2 using nitromethane as nitrogen source and their high photocatalytic performance', *Synth. React. Inorg. Metal-org. Nano-Metal Chem.*, 2015, **46**, pp. 766–774
[15] Samsudin E.M., Hamid S.B.A., Juan J.C., *ET AL.*: 'Effective role of trifluoroacetic acid (TFA) to enhance the photocatalytic activity of F-doped TiO_2 prepared by modified sol–gel method', *Appl. Surf. Sci.*, 2016, **365**, pp. 57–68
[16] Wang X.K., Wang C., Jiang W.Q., *ET AL.*: 'Sonochemical synthesis and characterization of Cl-doped TiO_2 and its application in the photodegradation of phthalate ester under visible light irradiation', *Chem. Eng. J.*, 2012, **189–190**, pp. 288–294

[17] Yang X., Cao C., Erickson L., *ET AL.*: 'Photo-catalytic degradation of rhodamine B on C-, S-, N-, and Fe-doped Tio_2 under visible-light irradiation', *Appl. Catal. B, Environ.*, 2009, **91**, pp. 657–662

[18] Ma D., Xin Y., Gao M., *ET AL.*: 'Fabrication and photocatalytic properties of cationic and anionic S-doped Tio_2 nanofibers by electrospinning', *Appl. Catal. B, Environ.*, 2014, **147**, pp. 49–57

[19] Gopal N.O., Lo H.H., Ke T.F., *ET AL.*: 'Visible light active phosphorus-doped TiO_2 nanoparticles: an EPR evidence for the enhanced charge separation', *J. Phys. Chem. C*, 2012, **116**, pp. 16191–16197

[20] Kong M., Li Y., Chen X., *ET AL.*: 'Tuning the relative concentration ratio of bulk defects to surface defects in Tio_2 nanocrystals leads to high photocatalytic efficiency', *J. Am. Chem. Soc.*, 2011, **133**, pp. 16414–16417

[21] Chen X., Liu L., Yu P.Y., *ET AL.*: 'Increasing solar absorption for photocatalysis with black hydrogenated titanium dioxide nanocrystals', *Science*, 2011, **331**, pp. 746–750

[22] Yan Y., Han M., Konkin A., *ET AL.*: 'Slightly hydrogenated Tio_2 with enhanced photocatalytic performance', *J. Mater. Chem. A*, 2014, **2**, pp. 12603–13170

[23] Wang G., Wang H., Ling Y., *ET AL.*: 'Hydrogen-treated Tio_2 nanowire arrays for photoelectrochemical water splitting', *Nano Lett.*, 2011, **11**, pp. 3026–3033

[24] Leshuk T., Parviz R., Everett P., *ET AL.*: 'Photocatalytic activity of hydrogenated Tio_2', *ACS Appl. Mater. Interfaces*, 2013, **5**, pp. 1892–1895

[25] Liu L., Yu P.Y., Chen X., *ET AL.*: 'Hydrogenation and disorder in engineered black TiO_2', *Phys. Rev. Lett.*, 2013, **111**, p. 65505

[26] Yu X., Kim B., Kim Y.K.: 'Highly enhanced photoactivity of anatase Tio_2 nanocrystals by controlled hydrogenation-induced surface defects', *ACS Catal.*, 2013, **3**, pp. 2479–2486

[27] Samsudin E.M., Hamid S.B.A., Juan J.C., *ET AL.*: 'Surface modification of mixed-phase hydrogenated TiO_2 and corresponding photocatalytic response', *Appl. Surf. Sci.* 2015, **359**, pp. 883–896

[28] Zhu G., Shan Y., Lin T., *ET AL.*: 'Hydrogenated blue titania with high solar absorption and greatly improved photocatalysis', *Nanoscale*, 2016, **8**, pp. 4705–4712

[29] Tian J., Leng Y., Cui H., *ET AL.*: 'Hydrogenated TiO_2 nanobelts as highly efficient photocatalytic organic dye degradation and hydrogen evolution photocatalyst', *J. Hazard. Mater.*, 2015, **299**, pp. 165–173

[30] Ramchiary A., Samdarshi S.K.: 'High visible light activity of hydrogenated structure-engineered mixed phase titania photocatalyst', *Chem. Phys. Lett.*, 2014, **597**, pp. 63–68

[31] Leshuk T., Linley S., Gu F.: 'Hydrogenation processing of TiO_2 nanoparticles', *Can. J. Chem. Eng.*, 2013, **91**, (5), pp. 799–807

[32] Das T.K., Ilaiyaraja P., Mocherla P.S.V., *ET AL.*: 'Influence of surface disorder, oxygen defects and bandgap in TiO_2 nanostructures on the photovoltaic properties of dye sensitized solar cells', *Sol. Energy Mater. Sol. Cells.*, 2016, **144**, pp. 194–209

[33] Cruz N.K.O., Semblante G.U., Senoro D.B., *ET AL.*: 'Dye degradation and antifouling properties of polyvinylidene fluoride/titanium oxide membrane prepared by sol-gel method', *J. Taiwan Inst. Chem. Eng.*, 2014, **45**, pp. 192–201

[34] Damodar R.A., You S.J.: 'Performance of an integrated membrane photocatalytic reactor for the removal of reactive black 5', *Sep. Purif. Technol.*, 2010, **71**, pp. 44–49

[35] Sharma S.K., Bhunia H., Bajpai P.K.: 'Photocatalytic decolorization kinetics and mineralization of reactive black 5 aqueous solution by UV/TiO_2 nanoparticles', *CLEAN, Soil Air Water*, 2012, **40**, pp. 1290–1296

[36] Zheng X., Li D., Li X., *ET AL.*: 'Photoelectrocatalytic degradation of rhodamine B on TiO_2 photonic crystals', *Phys. Chem. Chem. Phys.*, 2014, **16**, pp. 15299–15306

[37] Xing X., Xu Liu Y.W., Li Y., *ET AL.*: 'A one-step nonaqueous sol-gel route to mixed-phase Tio_2 with enhanced photocatalytic degradation of rhodamine B under visible light', *CrystEngComm*, 2016, **18**, pp. 1964–1975

[38] Liu W., Zhang Y.: 'Electrical characterization of $Tio_2/CH_3NH_3PbI_3$ heterojunction solar cells', *J. Mater. Chem. A*, 2014, **2**, pp. 10244–10249

[39] Xia T., Zhang W., Li W., *ET AL.*: 'Hydrogenated surface disorder enhances lithium ion battery performance', *Nano Energy*, 2013, **2**, pp. 826–835

[40] Xia T., Chen X.: 'Revealing the structural properties of hydrogenated black TiO_2 nanocrystals', *J. Mater. Chem. A*, 2013, **1**, pp. 2983–2989

[41] Jiang X., Zhang Y., Jiang J., *ET AL.*: 'Characterization of oxygen vacancy associates within hydrogenated TiO_2: a positron annihilation study', *J. Phys. Chem. C*, 2012, **116**, pp. 22619–22624

[42] Hu Y., Tsai H.L., Huang C.L.: 'Effect of brookite phase on the anatase-rutile transition in titania nanoparticles', *J. Eur. Ceram. Soc.*, 2003, **23**, pp. 691–696

[43] Bezrodna T., Gavrilko T., Puchkovska G., *ET AL.*: 'Spectroscopic study of TiO_2 (rutile) – benzophenone heterogeneous systems', *J. Mol. Struct.*, 2002, **614**, pp. 315–324

[44] Naldoni A., Allieta M., Santangelo S., *ET AL.*: 'Effect of nature and location of defects on bandgap narrowing in Black TiO_2 Nanoparticles', *J. Am. Chem. Soc.*, 2012, **134**, (8), pp. 7600–7603

[45] Huo J., Hu Y., Jiang H., *ET AL.*: 'In situ surface hydrogenation synthesis of Ti_3+ self-doped TiO2 with enhanced visible light photoactivity', *Nanoscale* 2014, **6**, (15), pp. 9078–9084

[46] Wang G., Xu L., Zhang J., *ET AL.*: 'Enhanced photocatalytic activity of TiO_2 powders (P25) via calcination treatment', *Int. J. Photoenergy* 2012, **2012**, pp. 1–9, Article ID 265760

[47] Mazinani B., Masrom A. K., Beitollahi A., *ET AL.*: 'Photocatalytic activity, surface area and phase modification of mesoporous SiO_2–TiO_2 prepared by a one-step hydrothermal procedure', *Ceram. Int.* 2014, **40**, (8), pp. 11525–11532

[48] Kim D.S., Han S.J., Kwak S.: 'Synthesis and photocatalytic activity of mesoporous TiO_2 with the surface area, crystallite size, and pore size', *J. Colloid Interface Sci.*, 2007, **316**, (1), pp. 85–91

[49] Xiang Q., Lv K., Yu J.: 'Pivotal role of fluorine in enhanced photocatalytic activity of anatase TiO_2 nanosheets with dominant (0 0 1) facets for the photocatalytic degradation of acetone in air', *Appl. Catal. B Environ.*, 2010, **96**, (3–4), pp. 557–564

[50] Yu J., Yu H., Cheng B., *ET AL.*: 'Enhanced photocatalytic activity of TiO_2 powder (P25) by hydrothermal treatment', *J. Mol. Catal. A Chem.*, 2006, **253**, (1–2), pp. 112–118

[51] Ibhadon A.O., Fitzpatrick P.: 'Heterogeneous photocatalysis: recent advances and applications', *Catalysts*, 2013, **3**, (1), pp. 189–218

[52] Zhang J., Zhou P., Liu J., Yu J.: 'New understanding of the difference of photocatalytic activity among anatase, rutile and brookite TiO_2', *Phys. Chem. Chem. Phys.*, 2014, **16**, (38), pp. 20382–20386

doi: 10.1049/mnl.2017.0238